Electromagnetic ion cyclotron waves in the subsolar region under normal dynamic pressure: Wind observations and theory

C. J. Farrugia,[1] G. Gnavi,[2] F. T. Gratton,[2] H. Matsui,[1] R. B. Torbert,[1] R. P. Lepping,[3] M. Oieroset,[4] and R. P. Lin[4]

[1] We analyze observations on electromagnetic ion cyclotron waves (EICWs) in the plasma depletion layer (PDL) made by Wind on three inbound passes of the magnetosheath near the stagnation streamline and model the observations using recent theory [*Gnavi et al.*, 2000]. While one pass was under substantially high solar wind dynamic pressure P_{dyn} ($\sim$6.4 nPa), two passes were under typical P_{dyn} at 1 AU ($\sim$2.2 nPa), which allows us to extend the study of EICWs into this lower pressure regime. Two passes were under steady, and one under time varying, conditions. We subdivide the PDL into inner, middle, and outer regions and compute in each the power spectral density (PSD) of the magnetic fluctuations transverse to the background field, using high-resolution ($\sim$11 samples/s) data from the Magnetic Field Investigation (MFI). The theory solves the kinetic dispersion relation in a plasma composed of electrons, protons, and α particles, each species modeled by bi-Maxwellian distribution functions. Results and trends indicated by the theory are found to be in qualitative agreement with the data. The observations show (1) at the inner PDL position the spectral PSD weakens as P_{dyn} decreases, and (2) the frequency range of emission shifts downward with diminishing P_{dyn}. Comparing observations with the classification of spectral types in the PDL under compressed conditions proposed by *Anderson et al.* [1994], we find a preponderance of so-called low and continuous spectra and only marginally bifurcated spectra with activity peaks below and above the alpha-resonance frequency. In general, as a consequence of smaller P_{dyn}, near the magnetopause our temperature anisotropies A_p are at the lower end of values characterizing bifurcated spectra in AMPTE/CCE. INDEX TERMS: 2728 Magnetospheric Physics: Magnetosheath; 2752 Magnetospheric Physics: MHD waves and instabilities; 2784 Magnetospheric Physics: Solar wind/magnetosphere interactions; 2753 Magnetospheric Physics: Numerical modeling; 2772 Magnetospheric Physics: Plasma waves and instabilities; KEYWORDS: plasma depletion layer (PDL), wave activity in PDL under normal conditions, wind passes near the stagnation streamline

1. Introduction

[2] The magnetic field in the Earth's magnetosheath is subject to a wide variety of fluctuations which change as the spacecraft proceeds from the bow shock to the magnetopause. In the main body of the magnetosheath, where the proton beta β_p is typically >1, the predominant magnetic fluctuations are longitudinal. Previous analyses have shown that these low-frequency ($\lesssim$100 mHz) compressive ($\Delta B/B \sim 1$) waves are mirror-mode waves [e.g., *Crooker and Siscoe*, 1977; *Anderson et al.*, 1994; *Denton et al.*, 1995; *Hill et al.*, 1995, and references therein]. As first noted by *Fairfield* [1976], close to the magnetopause, however, within the plasma depletion layer (PDL) [e.g., *Zwan and Wolf*, 1976; *Phan et al.*, 1994], where $\beta_p \lesssim 1$, the magnetic fluctuations become predominantly transverse to the background field and their frequency increases up to the proton gyrofrequency, f_p (0.1 to few Hz).

[3] Substantial progress in understanding these magnetic fluctuations and their evolution from the bow shock to the magnetopause was achieved with the AMPTE/CCE data set in both observational (see, e.g., *Anderson et al.* [1991, 1994], *Anderson and Fuselier* [1993], *Fuselier et al.* [1994], review by *Anderson* [1995], and theoretical and simulation work [*Gary et al.*, 1994a, 1994b, 1994c, 1997; *Denton et al.*, 1994, 1995]. Thus AMPTE/CCE researchers were able to

[1]Institute for the Study of Earth, Oceans, and Space, Space Research Center, and Department of Physics, University of New Hampshire, Durham, NH, USA.
[2]Instituto de Física del Plasma, CONICET and FCEyN-Universidad de Buenos Aires, Buenos Aires, Argentina.
[3]NASA Goddard Space Flight Center, Greenbelt, Maryland, USA.
[4]Space Science Laboratories, University of California, Berkeley, Berkeley, California, USA.

(1) show that the fluctuations in the PDL are mainly electromagnetic ion cyclotron waves (EICWs), with predominantly left-handed polarization at frequencies above 0.5 f_p; (2) demonstrate an anticorrelation between the proton thermal anisotropy, A_p ($A_p \equiv (T_\perp/T_\parallel) - 1$) and the proton beta parallel to the magnetic field, $\beta_{\parallel,p}$ ($\beta_{\parallel,p} \equiv 8\pi n_p T_\parallel/B^2$) [*Anderson and Fuselier*, 1993; *Anderson et al.*, 1994]; (3) catalogue five average magnetic spectral types corresponding to different locations in $A_p - \beta_\parallel$ space; (4) interpret the observed spectral types with the linear kinetic theory of the EICW microinstability [*Denton al.*, 1994]; and (5) derive the A_p versus $\beta_{\parallel,p}$ relation mentioned in 2 from nonlinear numerical simulations, proposing this anticorrelation as a closure formula for anisotropic magnetohydrodynamics in the PDL [e.g., *Gary et al.*, 1994c, 1997].

[4] As regards the five categories mentioned under 3, two are for compressional waves in the $\beta > 1$ magnetosheath and do not concern us here. Inside the PDL, three types of spectra were found, called respectively LOW, CON, and BIF. *Anderson et al.* [1994] define these categories as follows. (1) LOW, a continuous spectrum with the main power below f = 0.5 f_p and with comparable left and right hand power densities; (2) CON, a continuous spectrum with the main power starting from below 0.5 f_p and extending above 0.5 f_p. (3) BIF, bifurcated spectra with two broad peaks one above and one below 0.5 f_p separated by frequency gap with a net drop of power and with dominance of left-hand activity in the high-frequency range.

[5] All these studies refer to compressed magnetospheric conditions. The CCE spacecraft sampled the magnetosheath only when this boundary was earthward of spacecraft apogee at 8.8 R_E, corresponding to a solar wind dynamic pressure $P_{dyn} \geq 5.2$ nPa. This motivates our present work, which is to examine spectral features of EICWs in the PDL for a typical solar wind dynamic pressure at 1 AU of ~2 nPa. Comparison with the AMPTE-CCE results will thus isolate the role of P_{dyn} on the spectral classification. Further, a theory of these emissions which is applicable to normal P_{dyn} has been elaborated by *Gnavi et al.* [2000] (see below). Thus a final aim of this work is to compare observations with the theoretical predictions of *Gnavi et al.* [2000].

[6] These authors gave a theoretical description of EICW excitation along radial profiles in PDLs characterized by parameters from the superposed epoch analysis (SEA) of *Phan et al.* [1994], as explained next. Observations of the proton, electron, and magnetic field properties of the PDL under values of P_{dyn} more representative of usual solar wind P_{dyn} at 1 AU (historical average = 2.2 nPa) were carried out by AMPTE/IRM in thirteen passes of the low-shear magnetosheath made in 1984–1985 spanning 0800–1600 magnetic local times (MLT) and ±30° magnetic latitudes (MLAT) [*Paschmann et al.*, 1993; *Phan et al.*, 1994; see also *Phan and Paschmann*, 1995]. Average properties of the dayside PDL were compiled using a SEA technique by *Phan et al.* [1994]. SEA parameters reflect a lower average A_p together with a higher average $\beta_{\parallel,p}$ than those of the CCE studies.

[7] *Gnavi et al.* [2000] chose three key times referenced to the time of the magnetopause crossing, which they called "inner" (next to the magnetopause), "middle" (a position inside the PDL 5 min before the magnetopause crossing), and "outer" (10 min before the crossing). The main result

of this analysis was that in the inner region the proton contribution to EICW excitation is weaker than that at the middle and outer positions and that the α emission was dominant. In the middle and outer PDL the increasing β_p helps the proton emission to overcome the absorption due to the α particles in the proton frequency band so that both α and proton growth rate peaks are present in these regions. Gnavi et al. also studied features of the distribution functions that may merge the α and proton unstable bands, removing a possible power attenuation interval between them. Overall, the instability growth rates were found to be less intense than those obtained in the CCE studies, and they were mainly confined to frequencies below 0.5 f_p.

[8] In the present work we study EICW activity in the PDL using observations acquired on three radial, inbound passes by the Wind spacecraft near the subsolar line on 30 November 1994, 12 December 1994, and 24 December 1994. We chose these passes mainly because two levels of P_{dyn} were realized: P_{dyn} is ~2.2 nPa on 30 November 1994 and 12 December 1994 and ~6.4 nPa on 24 December 1994. We can thus analyze observations of EICWs in the PDL under more typical P_{dyn} and compare with theory.

[9] We describe our interpretational scheme and present the data in sections 2 and 3. In section 4 we study the power spectral densities (PSDs) using the highest resolution (11 samples/s) magnetic field data from Wind/MFI [*Lepping et al.*, 1995] and subdividing the PDL into three regions corresponding in steady cases to different distances from the magnetopause.

[10] We show first that EICWs are still present in the PDL even when solar wind P_{dyn} values are typical of normal conditions. We then analyze the changes in the power spectra which result from (1) distance from the magnetopause and (2) level of P_{dyn}. In section 5 we interpret the observations from the viewpoint of theory, basing ourselves on numerical solutions of the linear kinetic dispersion relation of EICWs. We input parameters measured on the three Wind passes. Since Wind did not measure alpha particles, we supplement the Wind data by AMPTE/CCE average values on α-particles [*Fuselier et al.*, 1991; *Denton et al.*, 1994]. In the discussion section 6, we compare our spectral features with those of *Anderson et al.* [1994], pointing out the weakening of EICW activity with the reduction of solar wind P_{dyn}.

2. Emission and Absorption of EICWs: Theory

2.1. Dispersion Relation

[11] We consider a plasma composed of electrons, protons, and α particles, all three modeled with bi-Maxwellian distribution functions of different parallel ($T_\parallel$) and perpendicular ($T_\perp$) temperatures, of the kind

$$f_{Max}^0 = \left(\frac{1}{\pi}\right)^{3/2} \frac{n}{w_\parallel w_\perp^2} \exp\left(-\frac{v_\parallel^2}{w_\parallel^2}\right) \exp\left(-\frac{v_\perp^2}{w_\perp^2}\right). \quad (1)$$

The spatio-temporal dependence of the waves is taken to be $\exp(i[kz - \omega t])$, with the z axis aligned along the background magnetic field B_0; k is the wave number; and $\omega = \omega_r + i\gamma$ is the complex frequency. Quantity $\omega_r = Re(\omega)$ is the angular frequency of the wave, and $\gamma = Im(\omega)$ is the

growth ($\gamma > 0$) or damping ($\gamma < 0$) rate. The species will be indexed by s ($s = p,\alpha,e$, for protons, alphas, and electrons, respectively). The relative density of the αs to the protons will be denoted by η_α. The quantity $w_{\parallel,s} = \sqrt{2k_B T_{\parallel,s}/m_s}$ is 'the thermal speed parallel to the magnetic field for each component. Similarly, $w_{\perp,s} = \sqrt{2k_B T_{\perp,s}/m_s}$ is the perpendicular thermal speed. The kinetic theory of plasma waves, based on the Vlasov self-consistent field model, leads to a linear dispersion equation for the waves. The dispersion relation for left-hand polarized EICWs, propagating along the magnetic field lines ($\vec{k} \parallel \vec{B}$), is given by

$$(kc)^2 = \omega^2 + \sum_s \omega_{p,s}^2 \left[A_s + \frac{(A_s + 1)\omega - A_s \Omega_s}{k w_{\parallel,s}} \right] Z_{0,s}\left(\frac{\omega - \Omega_s}{k w_{\parallel,s}} \right), \quad (2)$$

in which we write k instead of $k_\parallel$ for simplicity. (See, for example, Stix [1992] and Gary [1993] for a derivation). The sum extends over the species. The thermal anisotropy is $A_s = [(T_\perp/T_\parallel)_s - 1]$, $\omega_{p,s}$ stands for the plasma frequency, and Ω_s is the gyrofrequency for each species. Finally, Z_0 is the modified Plasma Zeta function [Stix, 1992], which takes into account both forward and backward propagating waves with respect to the orientation of the magnetic field.

[12] The numerical results given in the paper are based on a code we developed that solves the exact dispersion relation above. We compute the Z_0 function by power series expansion for small and moderate values of the argument, using quadratures for intermediate values (from the definition in terms of the error function of a complex argument) complemented by asymptotic expressions for large absolute values of the argument. The computation of Z_0 has been optimized and extensively controlled against a table of the Plasma Zeta function over the complex plane of the argument compiled by Fried and Conte [1961]. The code is coupled to an efficient commercial solver for implicit functions. Given a set of input parameters, we compute $\omega = \omega_r + i\gamma$ as a function of the real wavenumber k of the EIC waves and obtain both $\gamma = \gamma(k)$ and $\omega_r = \omega_r(k)$.

2.2. Resonant Emission of EICWs

[13] As discussed by Melrose [1986], to which we refer the reader for the derivations, an ion (proton or alpha particle) moving with a particular velocity component $v_\parallel^s$ ($s = p, \alpha$) along the field line, can only emit or absorb EICWs when the following resonance condition is satisfied:

$$\omega_r(k) - k v_\parallel^s = \Omega_s \quad (s = p, \alpha). \quad (3)$$

This equation means that the particle gyrates in concert with the transverse electric field of the wave at the Doppler-shifted frequency observed in the moving frame of the ion.

[14] The theory shows that for bi-Maxwellian distribution functions, the condition for wave growth, i.e., that there be more emitters than absorbers of a given ion species at any given frequency $\omega_r(k)$, can be written as

$$\frac{\overline{df_{0,s}}}{dv_\parallel}(v_\parallel^*) > 0, \quad (4)$$

where

$$\frac{\overline{df_{0,s}}}{dv_\parallel}(v_\parallel^*) \propto \left[\Omega_s \left(\frac{1}{w_{\parallel,s}^2} - \frac{1}{w_{\perp,s}^2} \right) - \frac{\omega_r(k)}{w_{\parallel,s}^2} \right] \overline{f_{0,s}}(v_\parallel^*). \quad (5)$$

Here, the function $\overline{f_{0,s}}(v_\parallel)$ is the bi-Maxwellian averaged over the perpendicular velocity $v_\perp$, and $v_\parallel^*$ is the peculiar $v_\parallel^s$ value that satisfies equation (3), $v_\parallel^* = (\omega_r(k) - \Omega_s)/k$, for each species. When the inequality in equation (4) is reversed, the wave is damped instead. As can be seen from equation (5), the number of emitters (or absorbers) at a given frequency of the wave, is proportional to

$$\exp\left[-\left((\omega_r(k) - \Omega_s)^2 / k^2 w_{\parallel,s}^2 \right) \right], \quad (6)$$

i.e., to the number of resonant ions. When $v_\parallel^*$ becomes suprathermal, $v_\parallel^* \gg w_{\parallel,s}$, few ions are left that can interact with the EICW.

[15] Equation (5) gives a frequency limit, ω_s^l, for each species, that separates the range of $\omega_r(k)$ in which the ions are predominantly emitters, $\omega_r < \omega_s^l$, from the range $\omega_r > \omega_s^l$, where the particles of that species absorb energy from the wave instead. The frequency limit for each species is given by

$$\omega_s^l = \frac{A_s}{A_s + 1} \Omega_s. \quad (7)$$

Since in our case $A_s > 0$, the frequency limit ω_s^l is smaller than the gyrofrequency of each ion component.

[16] As we examine increasing EICW frequencies, starting from $\omega_r = 0$, we find a low-frequency band in which both p and α are emitters and contribute to the growth of the waves. The rate of growth depends on the number of resonant ions, and it is negligibly small at very low frequencies, typical of the Alfvén wave regime. The rate of growth increases for higher frequencies approaching the alpha gyrofrequency Ω_α. However, before that value, the ω_α^l limit is found and thereafter, with increasing ω_r, the alpha particles produce absorption up to Ω_α and beyond.

[17] For frequencies higher than ω_α^l the protons keep generating growth until, with further increase of ω_r, we encounter their own limiting frequency ω_p^l. In the frequency interval between ω_α^l and ω_p^l there is a competition between absorption by α particles and emission by protons. The EICWs can either grow or damp down, depending on the number of interacting particles (equation (6)) of each species in that frequency range. Above that frequency, the protons too produce EICW damping and the wave intensity steadily declines.

[18] These features are described in Figures 1a and 1b, where the inequality, $\omega_\alpha^l < \omega_p^l$, corresponding to the most common anisotropy configurations, is assumed. These figures give a graphical representation to help visualize the mechanisms of wave growth or damping and to understand the numerical results of the theory presented later.

[19] We denote the dimensionless real frequency, the wave number, and the parallel velocity of a particle by

$$x = \frac{\omega_r}{\Omega_p}, \quad y = \frac{k V_A}{\Omega_p}, \quad u = \frac{v_\parallel}{w_\parallel}, \quad (8)$$

respectively, where $V_A \equiv B/\sqrt{4\pi m_p n_p}$ is the Alfvén velocity defined with the mass and the number density of
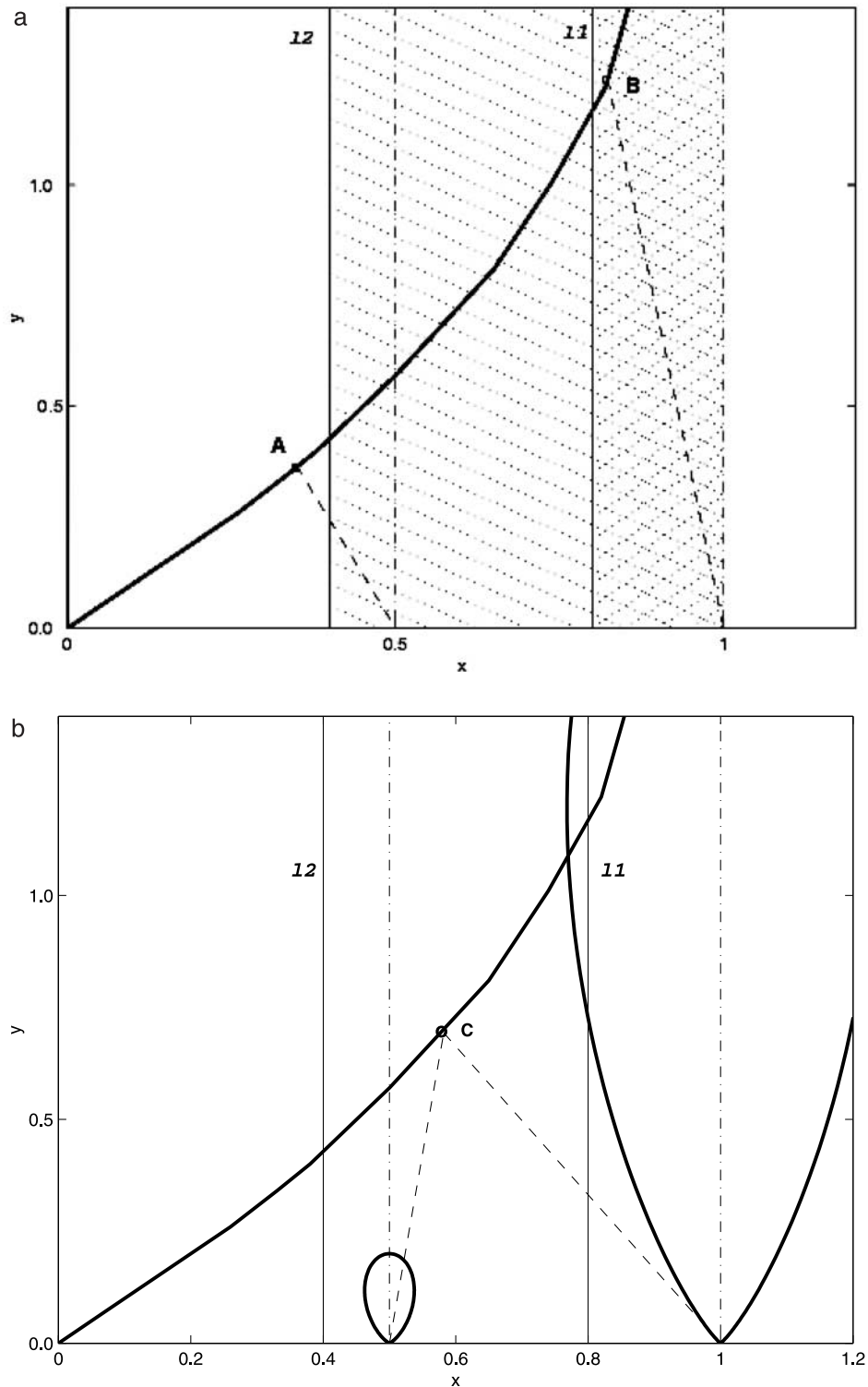
Figure 1. A schematic illustrating EIC wave-particle interactions. The plot format is wave number y versus frequency x, normalized as kV_A/Ω_p and ω_r/Ω_p, respectively. The solid trace in both panels gives the dispersion relation. The two solid vertical guidelines are the normalized limit frequencies l_2 and l_1, while the dashed vertical lines give the α and proton gyrofrequencies. The two points B and A in Figure 1a represent resonant conditions for the energy exchange of the wave with an α particle and a proton, respectively. Figure 1b shows a point C, whose frequency lies between l_2 and l_1, where two resonant lines intersect the dispersion relation. The additional contour lines (with respect to Figure 1a) qualitatively represent the distribution function for each species in a kind of polar display. As indicated by the contour lines, there are more α particles absorbing than there are protons emitting, leading to a net damping of the wave. For further details, see text.

the protons. Hence the dimensionless gyrofrequencies are 1 and 0.5, while the dimensionless limit frequencies are $l_1 = A_p/(A_p + 1)$ and $l_2 = A_\alpha/(A_\alpha + 1)$, for protons and αs, respectively. The particle resonant conditions are now

$$x = 1 + y\frac{u}{\sqrt{\beta_{p,\|}}}, \quad x = 0.5 + y\frac{u}{\sqrt{\beta_{\alpha,\|}}}, \quad (9)$$

for protons and αs, in that order. When plotted in a (x,y) plane these are straight lines inclined to the axis. In the y versus x plot of Figure 1, these lines pass through the points (1,0) or (0.5,0), with a slope dy/dx given by $\sqrt{\beta_{p,\|}}/u$ or $\sqrt{\beta_{\alpha,\|}}/u$, for protons and αs, respectively. Note that a proton resonates with a left EIC wave when its velocity u is negative (particle moving against the wave) (see Figure 1).

[20] In Figures 1a and 1b the solid curve $y = y(x)$, passing through the origin and approaching asymptotically the proton resonance at $x = 1$, represents the dispersion relation for the real part of the frequency of the EICWs. (The slope of $y(x)$ near the origin is unity, because these are Alfvén waves.) We have controlled that in all the cases examined in this paper the alpha resonance, present in a cold plasma dispersion relation, is entirely washed out by thermal effects. This is a known finite-beta effect that may happen in multicomponent ion plasmas for left EICWs [see, e.g., *Melrose*, 1986].

[21] In the same figure, the vertical dot-dashed lines represent the gyrofrequencies of protons and alpha particles, while the vertical solid lines indicate the positions of the limit frequencies, l_1 and l_2 ($l_2 < l_1$). The shaded area stretching from l_2 to 1 gives the frequencies where the α particles absorb. The hatched area between l_1 and 1 gives the frequencies where the protons, too, absorb. Thus enhanced absorption occurs in the hatched region, while between l_1 and l_2 the αs absorb and the protons emit, leading to a competition for energy transfer, which will be decided by the respective number of emitters (absorbers).

[22] Points A and B represent intersections of the resonant lines with the EICW dispersion relation, i.e., points in (xy) space where energy transfer takes place. At A a proton line crosses $y = y(x)$ and at that frequency the protons take up energy from the wave. Similarly, at B an α line crosses $y = y(x)$ and the alphas give up energy to the wave. The smaller the absolute value of the slope of these lines, the fewer the particles which take part in this transfer (the high energy tail of the distribution).

[23] An illustration of this point is given in Figure 1b. In this schematic, we have added two contours to represent the distribution functions of both species (αs on the left). The locus of each contour is made to vary with the velocity u, displaying qualitatively a polar representation of the distribution function, centered at the cyclotron frequency of each species. The polar angle (with respect to the y axis) varies with u, and the radial distance to the contour is proportional to the number of particles with that velocity. Two resonant lines are shown intersecting at point C, which lies in the frequency interval where energy exchange is determined by a competition between the protons and the αs. In this example the number of proton emitters is less than the number of alpha absorbers, as indicated in the figure. The

net result is a weakening of EICWs activity at this particular frequency.

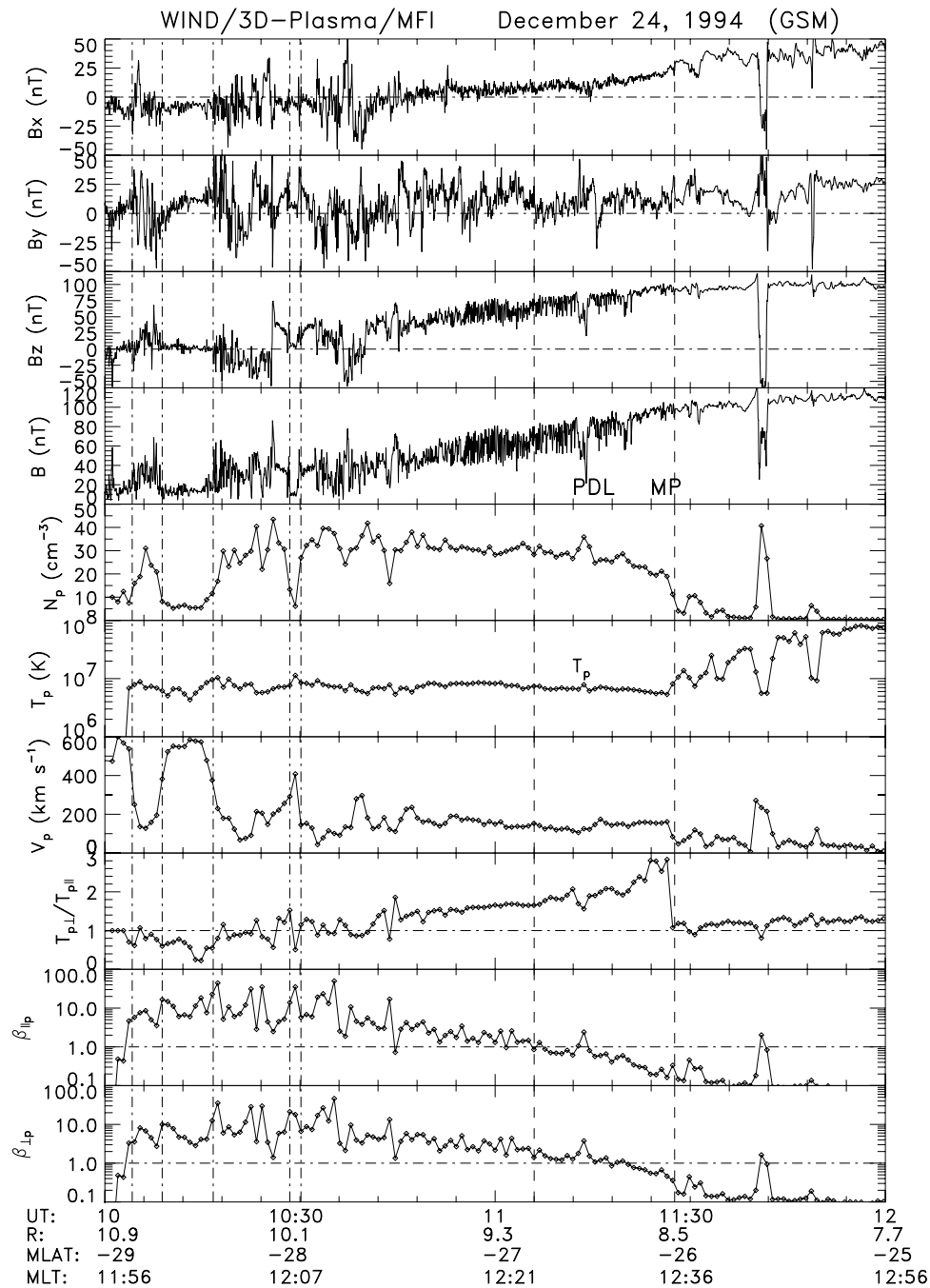## 3. Observations of PDLs by Wind Near the Stagnation Streamline

[24] Figures 2–4 display in the same format magnetic field and proton observations made by Wind on the three inbound magnetosheath passes on 24 December 1994 (Figure 2); 30 November 1994 (Figure 3); and 12 December 1994 (Figure 4). From top to bottom the panels show the GSM B_x, B_y, B_z components of the magnetic field, the total field, the proton density, temperature, and bulk speed, the temperature ratio $T_{p,\perp}/T_{p,\|}$, and the proton plasma betas parallel and perpendicular to the magnetic field. Electron data are available only on the 24 December 1994 pass (not shown) and indicate that in the magnetosheath the electron temperature is lower than the proton temperature by about a factor of 10, and the electron temperature ratio $T_{e,\perp}/T_{e,\|} \sim 1.1$. We may note that electron parameters have only a minor effect on EICW excitation [*Gnavi et al.*, 2000]. We shall henceforth assume the same T_e/T_p ratio of 24 December 1994 (=0.1) and temperature isotropy for the electrons on all passes. The magnetic field and plasma observations were made by the Magnetic Field Investigation (MFI) [*Lepping et al.*, 1995] and the 3-D Plasma Analyzer [*Lin et al.*, 1995] on Wind and are plotted at a resolution of 3 s and 51 s, respectively. The 0.09 s resolution magnetic field data are introduced later when we analyze the magnetic field fluctuations PSD in the PDL.

[25] Position data are shown at the bottom of each plot radial distance (R) in Earth radii (R_E), MLAT in degrees and MLT in hour:min. All passes are at low southern magnetic latitudes (MLAT) ranging from $-17°$ to $-29°$, and all passes take place within about 1 hour of local noon. We first discuss each pass in turn and then study the fluctuation spectra in the respective PDLs.

3.1. 24 December 1994

[26] The spacecraft starts in the fast (V $\sim$ 600 km s^{-1}) solar wind and encounters the bow shock at the times shown by first three vertical guidelines. Aside from a further, brief bow shock crossing at $\sim$1030 UT, shown between the fourth and fifth vertical guidelines, the spacecraft lies in the postnoon magnetosheath ($\sim$1220 MLT) until 1127 UT. Inside the magnetosheath the average density profile is flat or slowly decreasing up to 1106 UT, after which it commences a systematic decrease lasting 21 min. In this region, the average magnetic field strength increases steadily to 100 nT. At 1127 UT, the spacecraft crosses the magnetopause. At this crossing, the rotation of the field is just 15° [*Phan et al.*, 1996], making it a low-shear crossing. The sudden drop in the proton temperature ratio (panel 8), and the increase in T_p (panel 6) are both signatures of low-shear magnetopause crossings [*Paschmann et al.*, 1993]. Consistent with this interpretation is also the lower level of magnetic fluctuations of the magnetic field after 1127 UT, typical of the Earth's magnetosphere.

[27] We have defined the sunward edge of the PDL in the anisotropic magnetosheath as the location where $\beta_{p,\|} = 1$ [*Farrugia et al.*, 2000]. A vertical line has been drawn at this position (1106 UT, the second from right), and the

Figure 2. Magnetic field and proton observations made by Wind on an inbound magnetosheath pass near the stagnation streamline on 24 December 1994. From top to bottom the panels show the GSM B_x, B_y, B_z components of the magnetic field, the total field, the proton density, temperature, and bulk speed, the temperature ratio $T_{p,\perp}/T_{p,\parallel}$, and the proton plasma betas parallel and perpendicular to the magnetic field.

density decrease starts there. The region between the last two vertical guidelines is thus the PDL. One may note the decrease in T_p toward the magnetopause in the PDL, the small increase in V near the magnetopause, which *Phan et al.* [1996] showed to be consistent with stagnation line flow, the increase in the $T_{p,\perp}/T_{p,\parallel}$ ratio to a value of ∼3 at the magnetopause, which is the highest temperature anisotropy on the three passes, and the evident anticorrelation of $T_{p,\perp}/T_{p,\parallel}$ with $\beta_{p,\parallel}$ in the magnetosheath. In fact, from the point

when steady conditions prevailed (after 1042 UT), the $A_p(\beta_{p,\parallel})$ relation mentioned in the introduction is identical to that obtained by CCE experimenters [*Anderson et al.*, 1994], i.e., $A_p = 0.73\beta_{p,\parallel}^{-0.50}$.

[28] The magnetopause is crossed at a radial distance of 8.5 R_e. Ignoring the small offsets of the spacecraft trajectory from the stagnation streamline, and equating the stagnation point pressure to the magnetic pressure of a compressed dipole [*Spreiter et al.*, 1966], we obtain a solar wind
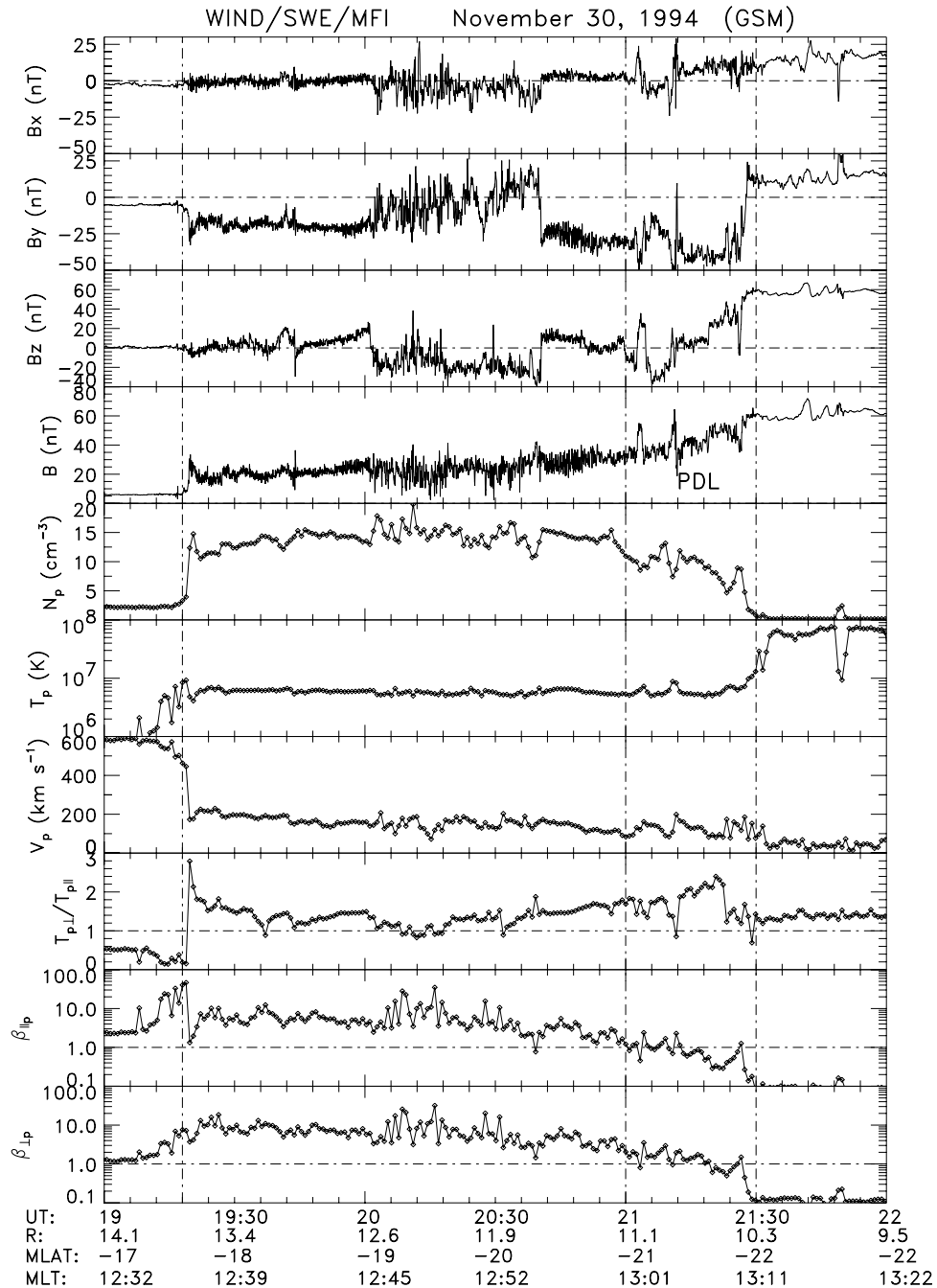
Figure 3. Similar to Figure 2 but for 30 November 1994.

dynamic pressure of ~6.4 nPa, corresponding to the lower values in the range of measured by AMPTE/CCE. This overlap with CCE observations facilitates later comparisons. (No simultaneous solar wind data are available on this or on the other two passes.)

[29] Well before the PDL is encountered, large fluctuations in the total field (panel 4) are evident, which affect mostly the major field component, B_z. These compressive field fluctuations with $\Delta B/B \sim 0.6$ have an average frequency of ~70 mHz and are mirror-mode waves. They persist with decreasing amplitude inside the sunward part of the PDL, but die out about 6 min before the magnetopause is encountered. Higher resolution field data discussed below

show that inside the PDL the power in the field fluctuations shifts to higher frequencies and resides mainly in the component transverse to the field.

3.2. 30 November 1994

[30] On this pass, the spacecraft starts in a steady and fast solar wind with the IMF oriented along the Parker spiral. It crosses into the magnetosheath at 1918 UT (first vertical guideline). Thereafter it traverses the postnoon magnetosheath (~1245 MLT), and reaches the magnetopause at 2130 UT.

[31] In contrast to the pass on 24 December 1994, the major field component in the magnetosheath is the east-west
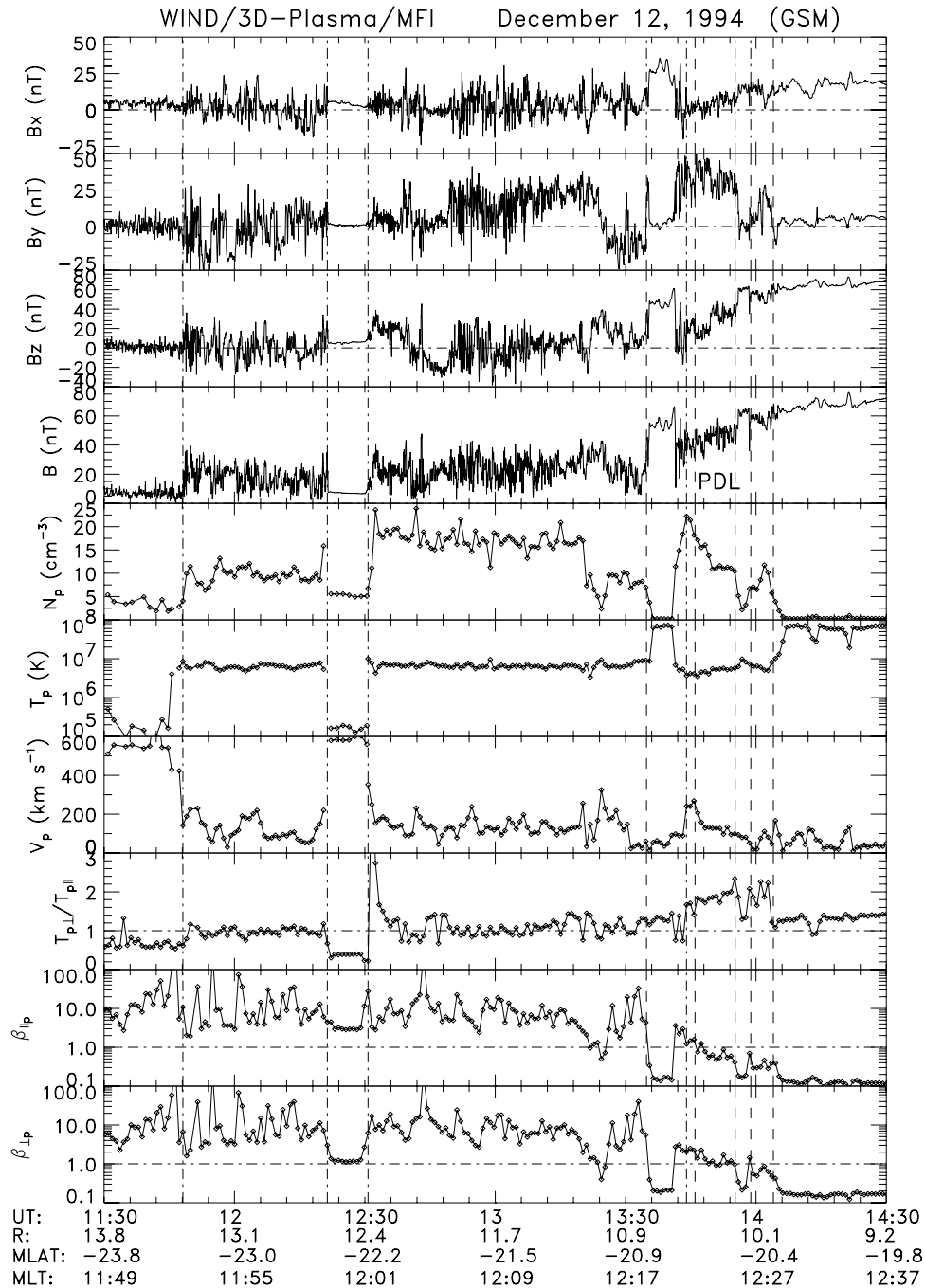
Figure 4. Similar to Figure 2 but for 12 December 1994.

component, B_y, which points predominantly west ($B_y < 0$). From 2002–2040 UT, a reorientation of the magnetosheath field occurs, where the field rotates south and east. This is a feature convected from the solar wind: IMP-8, which was located in the solar wind on the dawnside of the magnetosphere and tailward of Wind, observes this feature clearly (data not shown).

[32] The passage through the PDL occurs during the interval delimited by the last two vertical guidelines. The large drop in density, the increase in temperature, and the attenuation in the level of magnetic fluctuations signal the entry of the spacecraft into the magnetosphere at ~2130 UT at a radial distance of 10.31 R_E. Ignoring the

small offset of the spacecraft orbit from the subolar line and equating the stagnation pressure with the field pressure of a compressed dipole, as we did for 24 December, we obtain a solar wind dynamic pressure of 2.0 nPa (No simultaneous solar wind plasma data are available). Thus as on the 24 December 1994 pass, this pass is under fairly steady conditions, but, unlike it, the magnetosheath is sampled under typical solar wind pressure conditions (see section 1). This relatively uncompressed state is also partly responsible for the difference in the respective total magnetosheath field strengths at the magnetopause, that on 30 November (60 nT) being three-fifths the value on 24 December. Mirror mode waves are also present and

are of comparable frequency to those on 24 December ($\sim$80 mHz), with $\Delta B/B \approx 0.6$.

[33] The shear at the magnetopause is $\sim$40°, i.e., substantially higher than on 24 December. The magnetopause crossing may thus be classified as (borderline) high-shear [*Paschmann et al.*, 1993; *Phan et al.*, 1994]. In this respect, hints of enhanced flow speeds are present in the magnetopause current layer (near 2130 UT), which may be due to reconnection, but it is outside the scope of this paper to investigate these further. Nevertheless, as also found by CCE experimenters on magnetosheath passes for IMF $B_z < 0$ [see *Anderson et al.*, 1997, and references therein], there is a clear PDL. This starts at 2100 UT (when $\beta_{p,\parallel} = 1$) and continues up to the magnetopause crossing 30 min later, with a brief interruption at 2112 UT where a partial magnetopause crossing occurs. The plasma depletion is not as pronounced as on 24 December. Thus for example, the density at the inner edge of the PDL relative to values just behind the bow shock is smaller, the field compression is weaker, and the proton plasma beta is higher. As noted in section 1 and as suggested by the observations, this weaker PDL may be due to the fact that the advection of magnetic flux to the magnetopause is being partly counterbalanced by removal of flux by reconnection. An anticorrelation between the temperature anisotropy A_p and $\beta_{p,\parallel}$ is also present in the 30 November PDL, but the coefficients are different. We obtain $A_p = 0.29\beta_{p,\parallel}^{-0.32}$. In summary, 24 December and 30 November represent two quasi-steady passes under very different solar wind P_{dyn} conditions and somewhat different magnetic shear at the magnetopause.

3.3. 12 December 1994

[34] During the early part of the 12 December 1994 traversal of the magnetosheath, shown in Figure 4, Wind was downstream of a parallel shock; the IMF is mainly along the radial direction (x) and the Wind orbit straddles local noon. The high fluctuating level of the IMF contrasts sharply with that on 30 November. The bow shock is crossed three times, at 1148 UT, 2121 UT, and 2131 UT (first three vertical guidelines). By the time of the second bow shock crossing the IMF had acquired a positive B_z component with $B_z \approx B_x$. The shock is now quasi-perpendicular. It is also a stronger shock, as may be seen by the fourfold jump in density at $\sim$1230 UT.

[35] A first crossing of the magnetopause occurs at 1334 UT at a radial distance of 10.7 R_E (fourth vertical guideline). After that, the magnetopause retreats earthward, and from 1342 UT until 1404 UT the spacecraft is in a region where the field is progressively compressed and the density drops. Its outer edge is identified well by the $\beta_{p,\parallel} = 1$ criterion. A brief encounter with the magnetopause (1355–1359 UT) interrupts this PDL crossing. At the last magnetopause crossing (last vertical guideline) the magnetic shear is low ($\sim$20°).

[36] The degree of field compression and density depression in the PDL is comparable to that on 30 November 1994, as is also the level of dynamic pressure: 2.4 nPa is the value obtained at the time when the magnetopause is crossed last at a radial distance of $\sim$10.1 R_E. This is similar to the usual location of the subsolar magnetopause [*Fairfield*, 1971].

[37] We may summarize the major similarities and differences between the passes as follows. All passes are near the stagnation streamline. Both 24 December and 30 November are quasi-steady, whereas 12 December is nonsteady. Both 24 December and 12 December are low shear crossings of the magnetopause, while 30 November is marginally high shear. Nevertheless, even on 30 November, there was a clear depletion layer. Here 24 December was under compressed conditions, whereas the solar wind P_{dyn} on the other two passes was close to typical ($\sim$2.2 nPa). The temperature anisotropy and the level of depletion is strongest on 24 December. In all cases, A_p anticorrelates with $\beta_{p,\parallel}$. In all cases, the sunward edge of the PDL could be identified well by $\beta_{p,\parallel} = 1$. These being passes close to the stagnation streamline implies that the identification of the presence of a PDL by a systematic decrease in density (a result of MHD flow) [*Zwan and Wolf*, 1976] is particularly reliable since near the stagnation streamline gas dynamics would give a density increase instead [*Lees*, 1964].
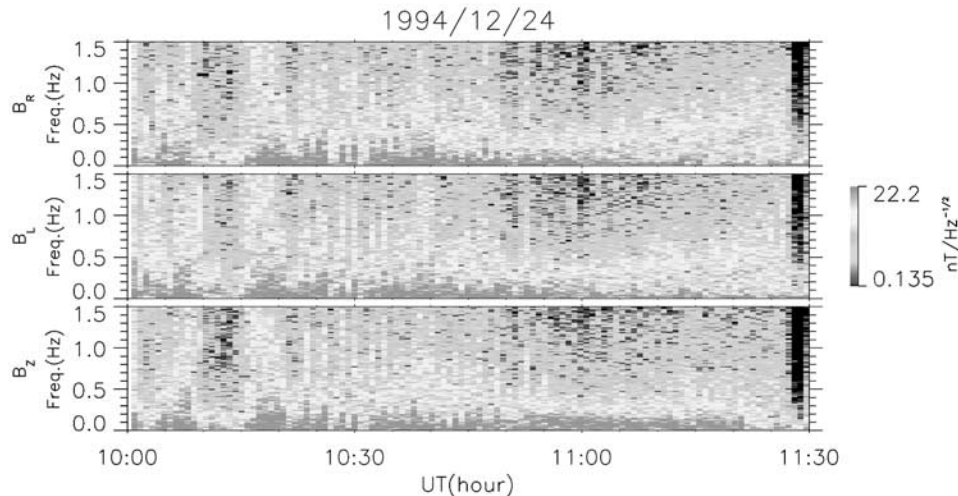
4. Magnetic Spectral Features
4.1. 24 December 1994

[38] Figure 5 shows spectrograms of the right (B_R), left (B_L), and parallel (B_Z) PSD of the fluctuations of the magnetic field. The horizontal scale is in decimal hours. The color scale for the PSD is given on the right. We use a moving field-aligned coordinate system computed every 90 s with adjacent data segments overlapped by 45 s. The period shown is from 1100 to 1130 UT and thus includes the magnetosphere starting from 1127 UT. The PDL is from 1106–1127 UT. Compressional power (B_Z) is evident at low frequencies up to $\sim$1126 UT, but in the PDL itself it resides only in the very low frequencies. As the magnetopause is approached, the spectrum at higher frequencies is dominated by the left and right hand fluctuations.

[39] We now subdivide the PDL into three regions, an inner (1122–1127 UT); middle (1116–1121 UT), and outer (1106–1111 UT) region. The proton parameters in these various regimes are given in Table 1, from which it can be seen that A_p is highest (lowest) and $\beta_\parallel$ is lowest (highest) in the inner (outer) regime. As anticipated in the introduction, the values of A_p are modest when compared to CCE average and individual values, and those of $\beta_\parallel$ are higher than AMPTE-CCE (see section 6 and *Anderson et al.* [1994]). The temperature anisotropy values on 24 December 1994 are the highest of the three passes.

[40] Figure 6 shows the PSD in each of these regimes for 24 December 1994. Plotted are the left-hand (heavy solid line), right hand (dot-dashed line), and parallel (dashed trace) PSDs. The vertical dot-dash lines in each panel give the proton and α-particle cyclotron frequencies. The vertical lines labeled L1 and L2 ($L1 > L2$) refer to the similarly labeled theoretical limiting frequencies discussed in section 2.2. Thus below frequency L2 (L1) the α particles (protons) give up energy to the wave; above L2 (L1) the alpha particles (protons) absorb energy from the wave. Between L2 and L1 there is a competition between the absorption of the alphas and the emission of the protons, and the direction of energy exchange depends on the value of the respective βs and the concentration of the alphas relative to the protons (see section 2.2). Figure 6 shows that frequencies L1 and L2 shift downwards as we go from inner to outer PDL regions.

Figure 5. A spectrogram of the right (B_R), left (B_L) and parallel (B_Z) power spectral density of the fluctuations of the magnetic field. The period shown is from 1100 to 1130 UT on 24 December 1994. The horizontal scale is in decimal hours. The color scale is given on the right. See color version of this figure at back of this issue.

[41] In the inner region, there is strong emission below $\sim$0.6 Hz in a band from $0.25-0.6$ Hz, i.e., extending up to $\sim$L2. Thereafter the spectral power decreases up to $\sim$0.73 Hz, where there is a much weaker emission band, which is below the L1 frequency and above the α gyrofrequency. At higher frequencies there is still some weak activity above L1. The first active band from $0.25-0.6$ Hz is due mainly to alpha emission. The secondary peak at 0.73 Hz is due to proton emission, which at a low $\beta_{p,\parallel} = 0.24$ and a moderate $A_p = 1.61$ (Table 1) is weaker than the α-peak.

[42] In the middle region, the main activity is below the L2 frequency at $\sim$0.2$-$0.4 Hz. A decrease sets in after that. There is a minor power enhancement just before and at the L1 frequency due to the protons, whereafter the power falls off approximately as a power law. For all frequencies above 0.2 Hz, the parallel power is lower and decreasing.

[43] In the outer region two power peaks, which just emerge from background, may be identified: the first is at 0.25 Hz, below the L2 frequency; the second, weaker power peak is at $\sim$0.42 Hz, below the L1 frequency. Note that this latter activity at a frequency intermediate between L1 and L2 is slightly stronger than the corresponding one in the middle region. This is because $\beta_{p,\parallel}$ is higher (=0.84) (Table 1), favoring more intense emission by the protons (see section 2.2).

4.2. 30 November 1994

[44] Figure 7 shows the PSD in the three regions of the PDL on 30 November 1994. The format is the same as

Figure 6. In the inner region it consists of two local power peaks straddling the alpha resonance. The first is at 0.25 Hz near L2 and the (weaker) second peak is at 0.43 Hz near L1. These enhanced powers are likely due to α and proton emissions, respectively.

[45] With respect to the inner region, the spectrum in the middle region is (1) shifted by $\sim$0.1 Hz to lower frequencies, and (2) the two power peaks have effectively merged. However, the PSD for frequencies between L1 and L2 is higher in this region due to the prevailing higher $\beta_{p,\parallel}$ (Table 1).

[46] In the outer region there appears to be continuous high power from 0.1 to $\sim$0.25 Hz. Thereafter the power drops sharply. Thus all the power resides in frequencies smaller than the α cyclotron frequency. Once again, between L2 and L1 the PSD increased because of the progressively increasing $\beta_{p,\parallel}$ from 0.3 to 1.13. Comparing the PSD for corresponding regions on 24 December, we see that there is significantly less wave power, i.e., weaker EICW activity, on 30 November and it is restricted to lower frequencies.

4.3. 12 December 1994

[47] Because of the time variability on this pass, the EICW evolution will be illustrated by subdividing into only two regions, the outer being after the magnetopause crossing and ending at 1346 UT and the inner before the final magnetosphere entry at 1349 UT. We recall that the designations "inner" and "outer" are made on the basis of the

Table 1. Parameters Used in the Computation of Theoretical Growth and Damping Rates (For Further Details, See Text)

| Day	Region	Duration	A_p	$\beta_{p\parallel}$	f_p	L_2	L_1
24 Dec 1994	Inner	$1122-1127$ UT	1.61 ± 0.23	0.24 ± 0.06	1.44 ± 0.05	0.50	0.89
	Middle	$1116-1121$ UT	1.05 ± 0.11	0.51 ± 0.11	1.29 ± 0.09	0.40	0.66
	Outer	$1106-1111$ UT	0.81 ± 0.08	0.84 ± 0.23	1.14 ± 0.08	0.33	0.51
30 Nov 1994	Inner	$2120-2123$ UT	1.25 ± 0.13	0.30 ± 0.02	0.77 ± 0.03	0.25	0.44
	Middle	$2113-2116$ UT	1.04 ± 0.12	0.69 ± 0.13	0.62 ± 0.04	0.19	0.32
	Outer	$2105-2108$ UT	0.66 ± 0.20	1.13 ± 0.28	0.56 ± 0.05	0.15	0.22
12 Dec 1994	Inner	$1352-1355$ UT	0.98 ± 0.02	0.66 ± 0.17	0.68 ± 0.07	0.21	0.33
	Outer	$1346-1349$ UT	0.80 ± 0.05	0.83 ± 0.29	0.66 ± 0.09	0.19	0.29
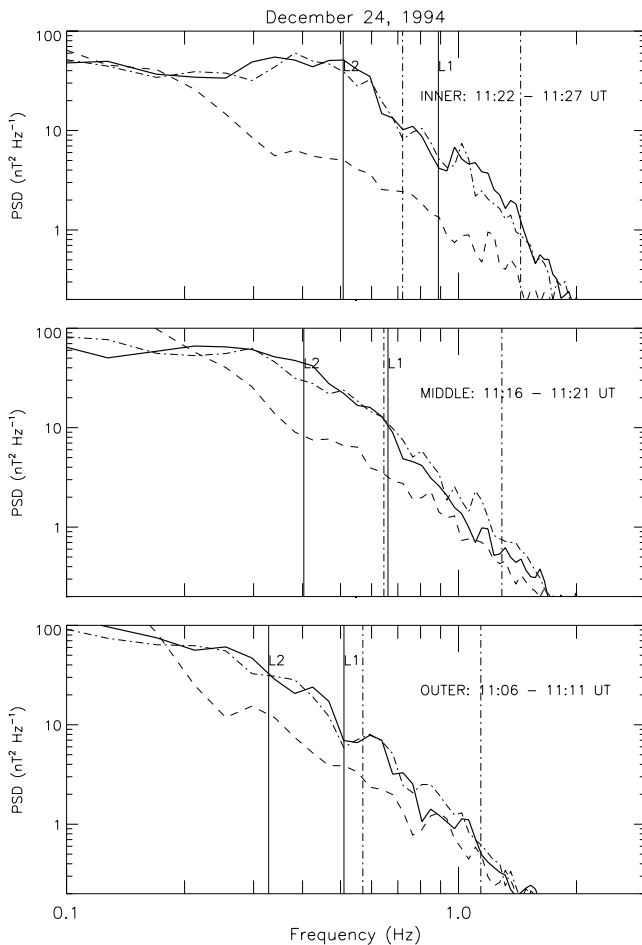
Figure 6. The figure shows the power spectral density (PSD) in the three subdivisions of the PDL (from top to bottom, inner, middle and outer) on 24 December 1994. Plotted are the left-hand (heavy solid line), right-hand (dot-dashed line) and parallel (dashed trace) PSDs. The vertical dot-dash lines in each panel give the proton and α-particle cyclotron frequencies, respectively. The vertical lines labeled L1 and L2 ($L1 > L2$) refer to the similarly-labeled theoretical limiting frequencies discussed in the text.

value of A_p, where in the "inner" region A_p is larger (0.98 versus 0.80) (Table 1). The respective spectra are shown in Figure 8.

[48] In the inner PDL (1352–1355 UT) the spectral power resides mainly at frequencies less than 0.21 Hz and in a much weaker band centered around the alpha resonance. In the outer PDL, continuously decreasing power is evident over the whole frequency range shown. Substantial power resides only in the range 0.1 to 0.25 Hz, well below the alpha resonance.

## 5. Growth and Damping Rates: Theory and Observations

[49] Figures 9–11 show the results of the numerical solutions of the dispersion relation (section 2.1). In a log-log format we plot for each pass the growth/damping rates, normalized to the proton gyrofrequency, versus the
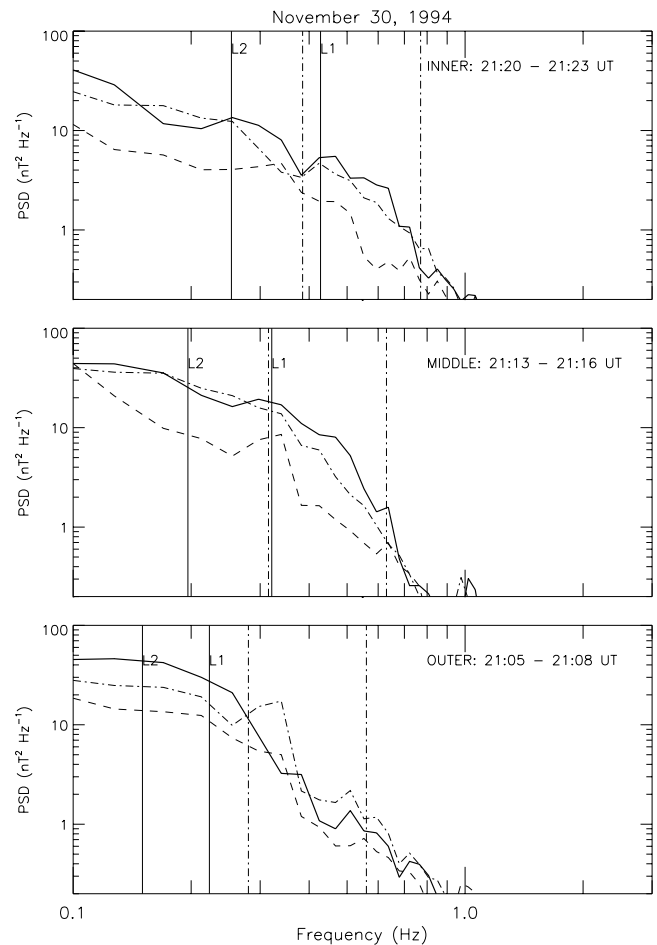
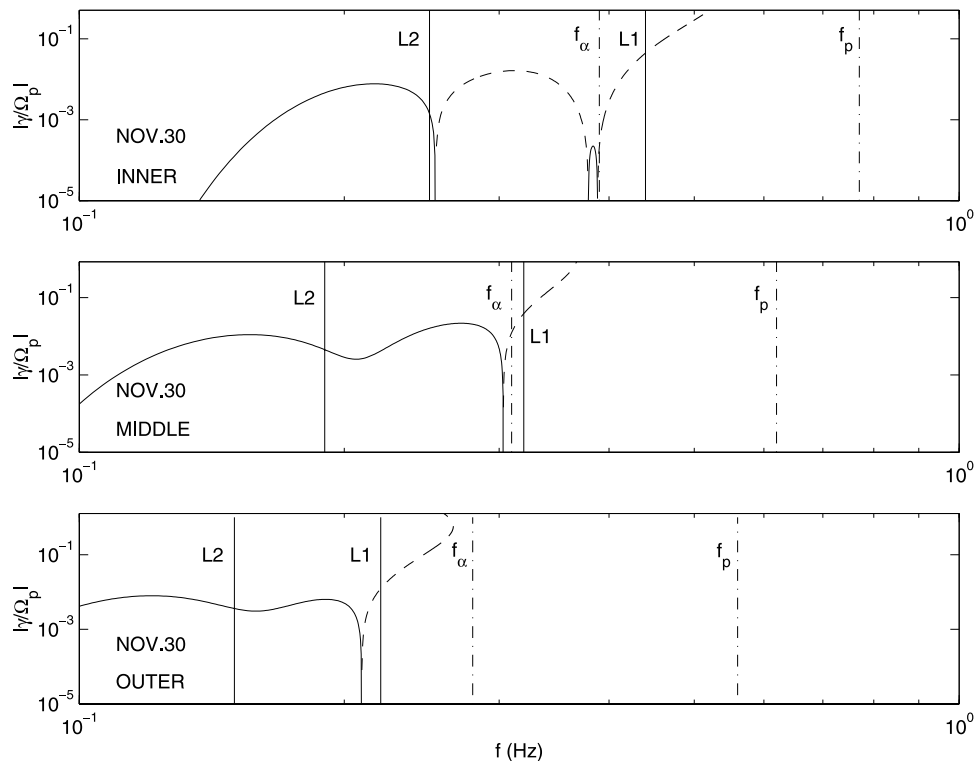**Figure 7.** Similar to Figure 6 but for 30 November 1994.
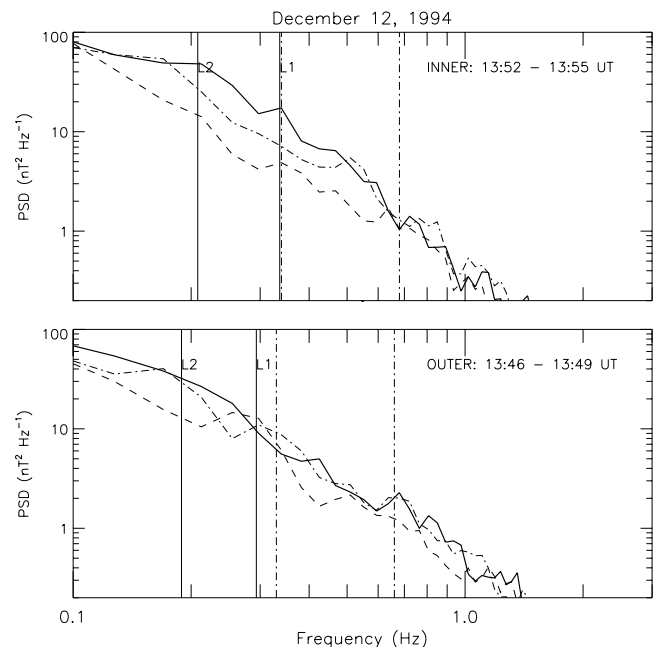
Figure 8. The PSDs in the inner and outer regions of the PDL encountered by Wind on 12 December 1994.
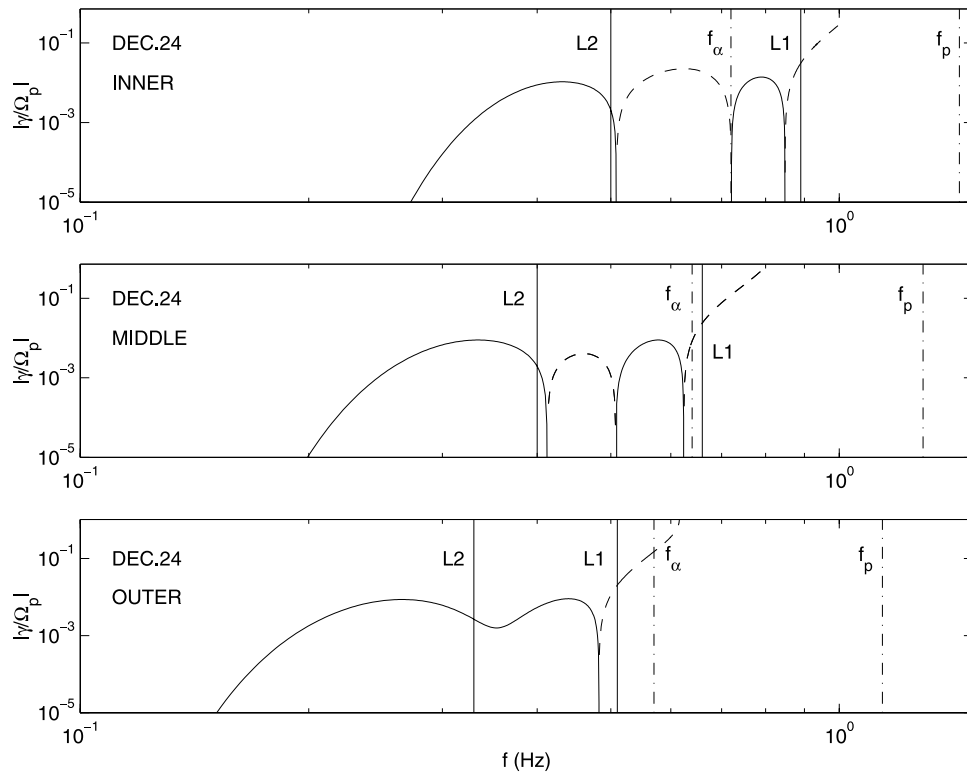
Figure 9. Theoretical growth rates as a function of frequency for the three regions of the PDL on 24 December 1994. The solid curves denote growth whereas the dashed curves denote damping rates. For further details see text.

frequency, f in Hz. The solid lines represent growth rates while the dashed lines refer to damping rates. The low-frequency range of EICWs with no lines plotted corresponds to the undamped Alfvén wave regime.

[50] As input to the calculations we need the parameters A_p, A_α, η_α, $\beta_{p,\parallel}$, $\beta_{\alpha,\parallel}$, β_e. Quantities A_p and $\beta_{p,\parallel}$ are averages over the subdivisions of the PDL taken from Wind measurements. Quantity η_α is assumed to be 0.04, a typical solar

Figure 10. Similar to Figure 9 but for 30 November 1994.
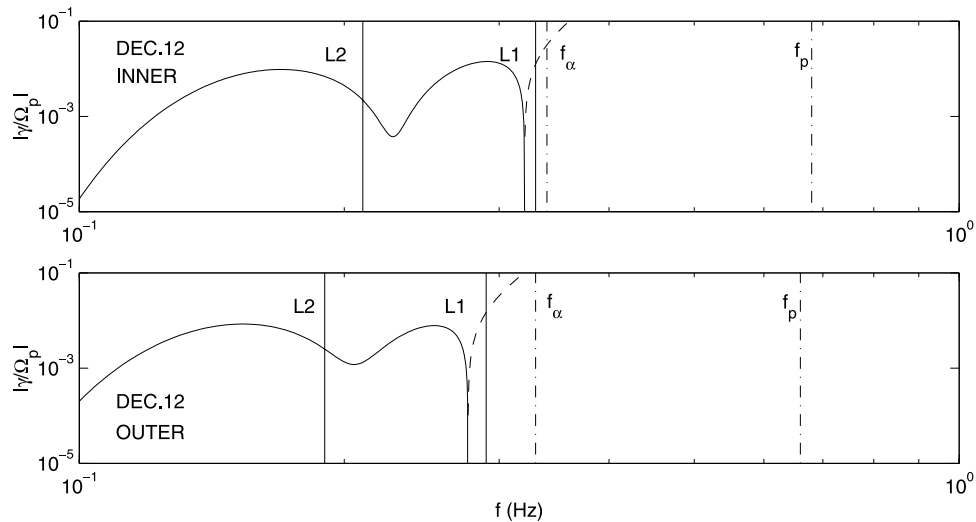
Figure 11. Similar to Figure 9 but for the two regions of the PDL on 12 December 1994.

wind value. The values of A_α and $\beta_{\alpha,\parallel}$ are taken from the literature. We set $T_\alpha/T_p = 4$ [*Anderson et al.*, 1991, and references therein]. For A_α, we assume $T_{\alpha,\perp}/T_{\alpha,\parallel} = 1.25 T_{p,\perp}/T_{p,\parallel}$, which agrees approximately with values measured by AMPTE-CCE [*Fuselier et al.*, 1991]. As mentioned earlier, the electrons are assumed to be isotropic and $T_p/T_e = 10$. The numerical values used are summarized in Table 1.

[51] As a general point, note that the height of the growth rate peaks that we present in these figures cannot be translated directly into power spectral peaks since the growth rate refers to the linear stage of the instability and does not characterize the saturation in the nonlinear regime, which is ultimately what Wind observes. However, the plots give the frequency ranges in which EICW excitation or damping occurs. *Gnavi et al.* [2000] studied linear mechanisms which can bridge apparent gaps in emission, leading to continuous spectra. Among these are (1) alpha-proton differential drifts, which have been seen in the magnetosheath [e.g., *Ogilvie et al.*, 1982], and (2) high A_α together with low $\beta_{p,\parallel}$. Although not treated here, it is to be expected that nonlinear interactions will generate new waves at frequencies that are stable according to linear theory. Thus complete agreement between linear theory and data should not to be expected.

5.1. 24 December 1994
5.1.1. Inner PDL
[52] Figure 9 shows the theoretical results in the top panel. Two activity ranges are seen, which are separated by a damped frequency band. The peak corresponding to the α emissions is centered at 0.42 Hz and extends from ~0.35 to 0.5 Hz. This excited frequency range agrees reasonably with the observations of Figure 6 (top panel). The second theoretical peak at 0.80 Hz, which is due to proton emission, is also present in the experimental power spectral densities at a frequency just below L1. Theory suggests a bifurcated spectrum that is, however, only weakly reflected in the data.

[53] The gap between ~0.50 Hz and ~0.72 Hz is damped at a rate comparable to the neighboring growth peaks.

Above ~0.85 Hz the damping becomes very strong, suppressing the high-frequency waves.
5.1.2. Middle PDL
[54] The theoretical results for the middle portion of the PDL are shown in the second panel of Figure 9. Theory predicts a broad alpha peak, centered at ~0.34 Hz, and the narrow proton peak centered at ~0.58 Hz. Looking at Figure 6, middle panel, we see that these theory features are reflected in the measured PSD as local enhancements at those frequencies. The gap between the two active frequency ranges resulting from theory is reproduced in the observed PSD only as a change in the slope of the spectrum just above the L2 frequency (see Figure 6, middle panel). Above ~0.62 Hz, the theoretical damping becomes very large. Correspondingly, in this high frequency domain measured PSD are very small.
5.1.3. Outer PDL
[55] In the outer PDL the theory predicts one continuous band of activity extending from 0.16 to 0.48 Hz, with an attenuation in growth rates at ~0.34 Hz. The two peaks have merged. The corresponding features in the observations are the two peaks at 0.26 Hz and 0.43 Hz (Figure 6, bottom panel). Beyond 0.5 Hz measured PSDs are very small except for a weak peak just above the L1 frequency. This latter feature is not predicted by theory.

[56] Finally, note that both theory and data show a shift to lower frequencies of the active band as we go from inner to outer PDL. This feature is also seen on all the passes.

5.2. 30 November 1994
5.2.1. Inner PDL
[57] Figure 10 shows the theoretical results. Both the α and proton emissions are seen, with the proton emission range being very narrow. They maximize at 0.24 Hz and 0.38 Hz, respectively. Near these frequencies the observed PSD shows local enhancements (see Figure 7, top panel), the lower frequency enhancement being broader. However, the theoretical frequency has a mismatch by about 0.05 Hz at the proton peak, the theoretical frequency being lower. There is damping between ~0.26–0.37 Hz, where the

observed PSD also declines. Beyond the proton activity peak the damping rates become increasingly stronger with increasing frequency.

5.2.2. Middle PDL

[58] In the middle PDL, the two active frequency ranges have merged, and a continuous active band stretches from 0.1 to 0.3 Hz. Between the activity peaks the growth rates are diminished, without being damped. Maximum growth rates are located at 0.15 Hz and 0.27 Hz for alpha and proton emissions, respectively. They have thus both moved to lower frequencies with respect to the inner PDL position. This trend, and the actual frequency at maximum growth, agree well with what is observed (see Figure 7, middle panel), where maximum spectral power is located at 0.15 and 0.22 Hz. Beyond the active range the damping rate increases very rapidly.

5.2.3. Outer PDL

[59] The theoretical growth rates form a continuous emission band ranging from below 0.1 to 0.22 Hz which does not extend above the α gyrofrequency. Thereafter the damping is extremely high. The low frequency continuous band of emission is also observed in the power spectral density (Figure 7, bottom panel). In the observations there is a sharp power decrease by about a factor of 10 starting at 0.25 Hz.

[60] In summary, for the low pressure pass on 30 November we find good agreement between the theory and the observations. For all three PDL regions, both in theory as well as in observations, the activity is shifted towards lower frequencies with respect to those of the high P_{dyn} pass on 24 December.

5.3. 12 December 1994

5.3.1. INNER and OUTER

[61] Figure 11 shows the theoretical results. For both inner and outer PDL regions the theoretical growths are very similar and both show continuous activity at low frequencies. In the inner region, the emission reaches up to 0.32 Hz, i.e., up to slightly below the alpha-resonance. With a cutoff at 0.28 Hz the active band in the outer PDL stops well short of the alpha resonance, exactly as in the data (see the kink in the spectrum at ~0.28 Hz) (Figure 8, bottom panel). At higher frequencies all theoretical wave emission in both regions is heavily damped. Thus theory predicts lack of activity above the alpha resonance for the outer, while some activity near the alpha resonance is predicted for the inner region of the PDL. To conclude this section, the linear theory of EICWs emission is in reasonable agreement with measured PSD for both high (24 December) as well as normal (30 November and 12 December) P_{dyn}.

6. Discussion

6.1. Comparison With AMPTE-CCE Studies

[62] As Table 1 shows, the observed values of the temperature anisotropy A_p on the Wind passes are significantly lower than those of the AMPTE-CCE measurements and the corresponding $\beta_{p,\parallel}$ are higher (compare our Table 1 with Table 2 of *Anderson et al.* [1994]).

[63] At lower values of P_{dyn} we expect the EICW activity to be weaker than at higher values for at least two reasons. (1) By producing lower A_p values, a smaller P_{dyn} generates conditions of smaller growth rates by weakening their driver (i.e., the free energy available). Further, excitation is pushed to lower frequencies, because frequencies L1 and L2 (measured in units of f_p) are shifted downwards. (2) Close to the (low-shear) magnetopause, $P_{dyn} \propto B^2$ (by pressure balance). Therefore a smaller P_{dyn} implies a smaller f_p (= $qB/2\pi mc$), which brings an additional diminution of the absolute values of the growth rates ($\propto f_p$) and the further shift of the EICW activity to lower frequencies).

[64] Thus a macroscopic solar wind quantity P_{dyn} has influence on a microinstability: the EICW activity in the PDL. We expect that some important differences will emerge when we compare our observational results with those of *Anderson et al.* [1994] and *Anderson and Fuselier* [1993]. Recall that AMPTE-CCE studies referred to compressed magnetospheric conditions with a solar wind P_{dyn} of the same order as, or larger than, our 24 December 1994 example. In contrast, our 30 November 1994 and 12 December 1994 passes were under typical P_{dyn} at 1 AU (~2.2 nPa).

[65] As mentioned in section 1, *Anderson and Fuselier* [1993] and *Anderson et al.* [1994] proposed a classification of magnetic spectral types in the magnetosheath. Inside the PDL the three identified categories were (1) bifurcated (BIF), (2) continuous (CON), and (3) low (LOW) spectra. In their statistical study (see Table 2 of *Anderson et al.* [1994]) the values of the parameters A_p and $\beta_{p,\parallel}$ characterizing the categories (averaged and standard deviation) are

	BIF	CON	LOW
$\langle A_p \rangle$	2.14 ± 0.25	0.96 ± 0.08	0.83 ± 0.05
$\langle \beta_{p,\parallel} \rangle$	0.22 ± 0.05	1.11 ± 0.18	1.25 ± 0.15

Thus $\langle A_p \rangle$ systematically increases (and correspondingly $\langle \beta_{p,\parallel} \rangle$ systematically decreases) from LOW to BIF spectra. According to *Anderson et al.* [1994] this progression implies a spatial classification.

[66] Following the same identifying criteria, our judgement as to which category our spectra belong to is as follows: 24 December (INNER) and 30 November (INNER) are BIF spectra; 24 December (MIDDLE and OUTER) and 30 November (MIDDLE) are CON spectra; 30 November OUTER and 12 December (INNER and OUTER) are LOW spectra. We note that our BIF cases are only marginally so in that, for example, the secondary (proton) peak in transverse power hardly shows a broad local maximum (contrast Figures 6 and 7, upper panels, with Figure 1, last panel in the work of *Anderson et al.* [1994]). The passes on 24 December and 30 November were steady, and thus our results corroborate directly the view that these spectral types correspond to a spatial classification. That is, our subdivisions reflect a bona fide spatial structuring of the PDL in terms of wave activity, which extends even to normal P_{dyn}.

[67] As regards the actual values of $\langle A_p \rangle$ measured by Wind, our LOW and CON varieties have values of $\langle A_p \rangle$ (0.81 ± 0.16 (LOW) and 0.97 ± 0.14 (CON); three spectra each) lying close to the average values in the *Anderson et al.*

[1994] classification of these types (0.83 ± 0.05 (LOW) and 0.96 ± 0.08 (CON); see their Table 2). However, our two BIF spectra have $A_p = 1.61$ (24 December 1994) and 1.30 (30 November 1994), which are well below the average values of *Anderson et al.* [1994] (= 2.14 ± 0.26) and correspond to the lower end of the scale of values in their bifurcated category. We believe that this is due to the lower P_{dyn}. The $\langle \beta_{p,\parallel} \rangle$ for LOW and CON spectra are, however, higher than those of *Anderson et al.* [1994] (0.87 ± 0.24 (LOW), 0.68 ± 0.17 (CON)), and thus the $A_p - \beta_{p,\parallel}$ relation for 30 November and 12 December 1994 has different coefficients than those of *Anderson et al.* [1994]. As a consequence of these comparisons, we predict that under normal solar wind dynamic pressure there will be a preponderance of spectra of the CON and LOW types in the PDL, and few BIF spectra, if any. We also expect weaker EICW activity in the PDL than under compressed conditions.

6.2. Comparison With Theory

[68] *Gnavi et al.* [2000] based their theoretical predictions on EICW generation in the PDL on SEA parameters (see section 1), which, while referring to more typical solar wind P_{dyn}, are averages over many passes. The computations reported in section 5 are for proton properties as measured on the three passes we study here. The α-properties (η_α, A_α, and β_α are the same as in the present computations and are taken from the literature (section 5). The agreement of several features of the power spectral densities with theoretical results was qualitatively good. The theory and observations agreed on the frequency where the activity peaks. The consequence of the width of the active bands, and the effects related to the limiting frequencies L2 and L1, particularly the strong power decrease at frequencies larger than the latter, were observed. Finally, we note that both theory and observations show a shift to lower frequencies of the active band as we go from inner to outer PDL regions. This is a feature seen on all passes.

[69] There were also some discrepancies which may have various origins. Exact comparisons were hindered by the absence of actual measurements of the properties of the alpha properties. On the theoretical side, there are nonlinear effects, such as parametric decays and turbulent cascades, which were not studied here. There is also a general shortcoming common to all infinite plasma models for PDL waves which assume a spatial uniformity of properties, which is never realized in practice.

[70] *Gnavi et al.* [2000] were the first to suggest the subdivision of the PDL. In this way evolutionary trends of the EICWs excitation were exposed. We see these evolutionary trends in the data of the WIND passes, which justifies the subdivision a posteriori.

[71] Summing up, we have documented and analyzed for the first time the presence of EICWs in the terrestrial PDL under normal ($\sim$2.2 nPa) solar wind dynamic pressure. We have extended the analysis of EICW spectra and theory comparisons to this more typical P_{dyn} regime.

References

Anderson, B. J. (1995), ULF signals observed near the magnetopause, in *Physics of the Magnetopause, Geophys. Monog. Ser.*, vol. 90, edited by P. Song, B. U. Sonnerup, and M. F. Thomsen, p. 269, AGU, Washington, D.C.

Anderson, B. J., and S. A. Fuselier (1993), Magnetic pulsations from 0.1 to 4 Hz and associated plasma properties in the Earth's subsolar magnetosheath and plasma depletion layer, *J. Geophys. Res.*, 98, 1461.

Anderson, B. J., S. A. Fuselier, and D. Murr (1991), Electromagnetic ion cyclotron waves observed in the plasma depletion layer, *Geophys. Res. Lett.*, 18, 1955.

Anderson, B. J., S. A. Fuselier, S. P. Gary, and R. E. Denton (1994), Magnetic spectral signatures in the Earth's magnetosheath and plasma depletion layer, *J. Geophys. Res.*, 99, 5877.

Anderson, B. J., T.-D. Phan, and S. A. Fuselier (1997), Relationships between plasma depletion and subsolar reconnection, *J. Geophys. Res.*, 102, 9531.

Crooker, N. U., and G. L. Siscoe (1977), A mechanism for pressure anisotropy in the subsonic magnetosheath region, *J. Geophys. Res.*, 82, 185.

Denton, R. E., S. P. Gary, B. J. Anderson, S. A. Fuselier, and M. K. Hudson (1994), Low-frequency magnetic fluctuation spectra in the magnetosheath and plasma depletion layer, *J. Geophys. Res.*, 99, 5893.

Denton, R. E., S. P. Gary, X. Li, B. J. Anderson, J. W. LaBelle, and M. Lessard (1995), Low-frequency fluctuations in the magnetosheath near the magnetopause, *J. Geophys. Res.*, 100, 5665.

Fairfield, D. H. (1971), Average and unusual locations of the Earth's magnetopause and bow shock, *J. Geophys. Res.*, 76, 6700.

Fairfield, D. H. (1976), Waves in the vicinity of the magnetopause, in *Magnetospheric Particles and Fields*, pp. 67, edited by B. M. McCormac, D. Reidel, Norwell, Mass.

Farrugia, C. J., N. V. Erkaev, and H. K. Biernat (2000), On the effects of solar wind dynamic pressure on the anisotropic magnetosheath, *J. Geophys. Res.*, 105, 115.

Fried, D. B., and S. D. Conte (1961), *The Plasma Dispersion Function*, Academic, San Diego, Calif.

Fuselier, S. A., D. M. Klumpar, E. G. Shelley, B. J. Anderson, and A. Coates (1991), He^{2+} and H^+ dynamics in the subsolar magnetosheath and plasma depletion layer, *J. Geophys. Res.*, 96, 21,095.

Fuselier, S. A., B. J. Andersen, S. P. Gary, and R. E. Denton (1994), Inverse correlations between the ion temperature anisotropy and the plasma beta in the Earth's quasi-parallel magnetosheath, *J. Geophys. Res.*, 99, 14,931.

Gary, S. P. (1993), *Theory of Space Plasma Microinstabilities*, Cambridge Univ. Press, New York.

Gary, S. P., M. E. McKean, D. Winske, B. J. Anderson, R. E. Denton, and S. A. Fuselier (1994a), The proton cyclotron instability and the anisotropy/beta inverse correlation, *J. Geophys. Res.*, 99, 5903.

Gary, S. P., R. D. Convery, R. E. Denton, S. A. Fuselier, and B. J. Anderson (1994b), Proton and helium cyclotron anisotropy instability thresholds in the magnetosheath, *J. Geophys. Res.*, 99, 5915.

Gary, S. P., B. J. Anderson, R. E. Denton, S. A. Fuselier, and M. E. McKean (1994c), A limited closure relation for anisotropic plasmas in the Earth's magnetosheath, *Phys. Plasmas*, 1, 1676.

Gary, S. P., J. Wang, D. Winske, and S. A. Fuselier (1997), Proton temperature anisotropy upper bound, *J. Geophys. Res.*, 102, 27,159.

Gnavi, G., F. T. Gratton, and C. J. Farrugia (2000), Theoretical properties of electromagnetic ion cyclotron waves in the terrestrial, dayside, low latitude plasma depletion layer under uncompressed magnetosheath conditions, *J. Geophys. Res.*, 105, 20,973.

Hill, P., G. Paschmann, R. A. Treumann, W. Baumjohann, N. Sckopke, and H. Luehr (1995), Plasma and magnetic field behavior across the magnetosheath near local noon, *J. Geophys. Res.*, 100, 9575.

Lees, L. (1964), Interaction between the solar wind plasma and the geomagnetic cavity, *AIAA J.*, 2, 1576.

Lepping, R. P., et al. (1995), The Wind Magnetic Field Investigation, *Space Sci. Rev.*, 71, 207.

Lin, R. P., et al. (1995), A three-dimensional plasma and energetic particle investigation for the Wind spacecraft, *Space Sci. Rev.*, 71, 125.

Melrose, D. B. (1986), *Instabilities in Space and Laboratory Plasmas*, Cambridge Univ. Press, New York.

Ogilvie, K. W., M. A. Coplan, and R. D. Zwickl (1982), Helium, hydrogen and oxygen velocities observed on ISEE 3, *J. Geophys. Res.*, *87*, 7363.

Paschmann, G., W. Baumjohann, N. Sckopke, T.-D. Phan, and H. Lühr (1993), Structure of the dayside magnetopause for low magnetic shear, *J. Geophys. Res.*, *98*, 13,409.

Phan, T.-D., and G. Paschmann (1995), The magnetosheath region adjacent to the dayside magnetopause, in *Physics of the Magnetosphere*, *Geophys. Monogr. Ser.*, vol. 90, edited by P. Song, B. U. O. Sonnerup, and M. F. Thomsen, p. 115, AGU, Washington, D. C.

Phan, T.-D., G. Paschmann, W. Baumjohann, N. Sckopke, and H. Luehr (1994), The magnetosheath region adjacent to the dayside magnetopause: AMPTE/IRM Observations, *J. Geophys. Res.*, *99*, 121.

Phan, T.-D., et al. (1996), The subsolar magnetosheath and magnetopause for high solar wind ram pressure: WIND observations, *Geophys. Res. Lett.*, *23*, 1279.

Spreiter, J. R., A. L. Summers, and A. Y. Alksne (1966), Hydromagnetic flow around the magnetosphere, *Planet. Space Sci.*, *14*, 223.

Stix, H. T. (1992), *Waves in Plasmas*, Am. Inst. of Phys., New York.

Zwan, B. J., and R. A. Wolf (1976), Depletion of solar wind plasma near a planetary boundary, *J. Geophys. Res.*, *81*, 1636.

————————————

C. J. Farrugia, H. Matsui, and R. B. Torbert, Space Science Center, University of New Hampshire, Morse Hall, Room 414, Durham, NH 03824, USA. (charlie.farrugia@unh.edu; hiroshi.matsui@unh.edu)

G. Gnavi and F. T. Gratton, Instituto de Física del Plasma, CONICET and FCEyN, Universidad de Buenos Aires, 1428 Buenos Aires, Argentina. (gracielagnavi@infip.org; faustogratton@infip.org)

R. P. Lepping, Laboratory for Extraterrestrial Physics, NASA Goddard Space Flight Center, Greenbelt, MD 20771, USA. (ron.lepping@gsfc.nasa.gov)

R. P. Lin and M. Oieroset, Space Science Laboratory, University of California, Berkeley, Berkeley, CA 94720, USA. (rlin@ssl.berkeley.edu; oieroset@ssl.berkeley.edu)

Figure 5. A spectrogram of the right (B_R), left (B_L) and parallel (B_Z) power spectral density of the fluctuations of the magnetic field. The period shown is from 1100 to 1130 UT on 24 December 1994. The horizontal scale is in decimal hours. The color scale is given on the right.